

Building Damage Detection of the 2010 Haiti Earthquake Based on Texture Analysis of High-Resolution Satellite Images

H. Miura, S. Midorikawa, and H.-C. Soh

Department of Built Environment, Tokyo Institute of Technology, Japan



SUMMARY:

In order to develop an automatic damage detection methodology, the characteristics of building damage areas in high-resolution satellite images observed before and after the 2010 Haiti earthquake are examined. From the texture analysis based on gray-level co-occurrence matrix, the dissimilarity of the images is identified as better classifier than other texture indices in detecting collapsed buildings. By using the dissimilarity calculated from the pre- and post-event images, damage detection is performed to identify the distribution of the collapsed buildings and the accuracy of the detection is assessed by the ROC analysis. The result shows that about 70% of the collapsed buildings are correctly detected by the proposed method.

Keywords: Damage detection, Texture analysis, High-resolution satellite image, The 2010 Haiti earthquake

1. INTRODUCTION

In a destructive earthquake, buildings and infrastructures would be severely damaged over a wide area. For planning early stage relief and recovery efforts, it is essential to identify building damage distribution immediately after the earthquake. Remotely sensed images have been employed to assess the building damage in recent large earthquakes because the images can quickly capture the real world from space at a time.

In the Haiti earthquake (M_w 7.0) on 12 Jan. 2010, more than 300,000 were killed, about 105,000 houses were totally destroyed and over 208,000 homes were damaged (Government of the Republic of Haiti, 2010). After the earthquake, remote sensing-based damage assessments were performed using high-resolution satellite images and aerial photographs (e.g., Ghosh et al., 2011). However, since the building damage was visually identified by crowdsourced volunteers, many human resources were required to obtain the building damage map. To quickly obtain the damage map with less labor, it is necessary to develop a methodology for automatically detecting the damage areas by an image analysis technique.

Image texture analyses have been used for automatic or semi-automatic damage detection from high-resolution satellite images (Huyck et al., 2005; Rathje et al., 2005). They estimated the 50m to 100m-mesh based damage distributions by the texture analysis and compared to visually interpreted damage maps. However, the textural characteristics of individual damaged and undamaged buildings and the detection accuracy for each building have not been fully discussed. In this study, the characteristics of image texture in damaged buildings are examined using high-resolution satellite images observed before and after the 2010 Haiti earthquake and building-by-building damage data. The texture analysis is performed to automatically detect collapsed buildings and the detection accuracy is assessed.

2. SATELLITE IMAGES AND DAMAGE DATA

In Port-au-Prince, the capital of the republic of Haiti, huge number of buildings was severely damaged

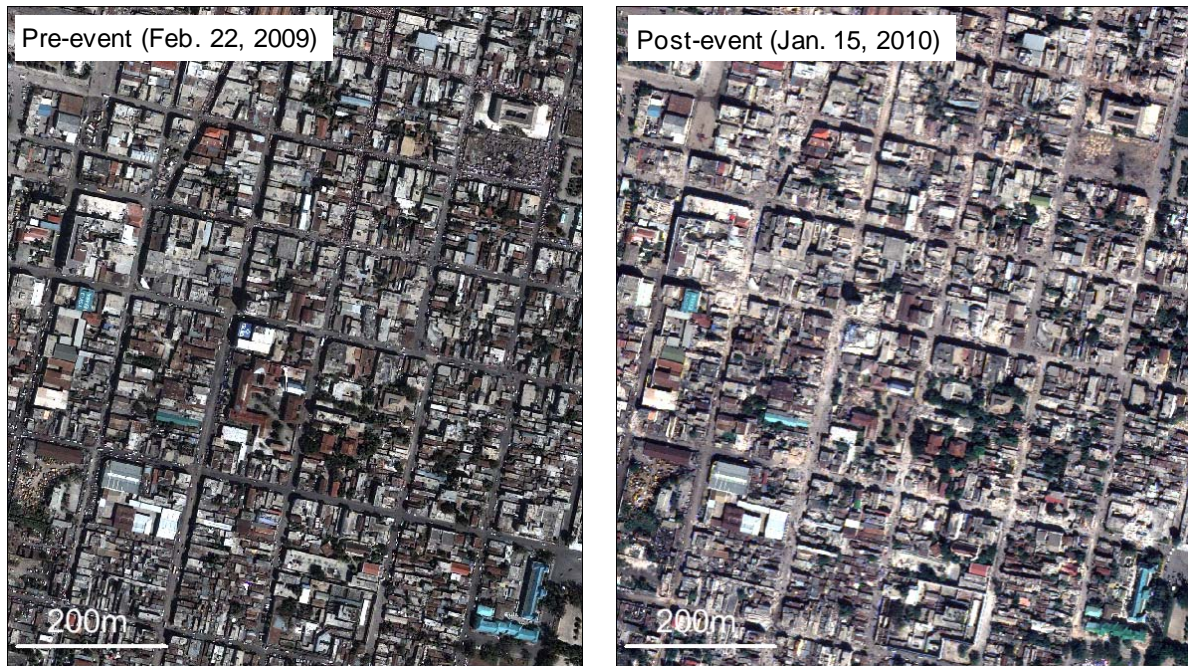


Fig. 1 Pre- and post-event high-resolution satellite images

in the 2010 Haiti earthquake. A built-up area in Port-au-Prince is selected as the target area of this study. High-resolution satellite optical images observed before and after the earthquake are used in the analysis. Quick Bird (QB) image with the spatial resolution of 0.6m and WorldView-2 (WV) image with the resolution of 0.5m are used as pre- and post-event image, respectively. Although the use of same resolution images is preferable for digital analysis of two images, pre-event WV image is not available because the WV satellite has just launched in Oct. 2009. The both images consist of four bands namely blue, green, red and near infrared band. Figure 1 shows the pan-sharpened pre- and post-event images in the target area extending about 850m and 750m for NS and EW directions, respectively.

In order to examine the relation between the image characteristics and building damage, building damage data is used. The UNISTAR/UNOSAT created building damage data by visual interpretation of high-resolution satellite images and aerial photos observed after the earthquake (UNISTAR/UNOSAT, 2010). The data includes the geo-referenced point data for all the buildings in Port-au-Prince with the damage level classified to four categories based on EMS-98; G5: Collapse, G4: Severe damage, G3: Moderate damage and G1: Negligible damage. In order to examine the spatial characteristics of the images for each damaged building, the building footprints are delineated from the images and the damage levels are attributed to the footprints. The building footprint data with the damage level is used as the damage data in this study. Figure 2 shows the distribution of damage data in the target area. The area covers totally 1378 buildings including 508 G5 buildings that correspond to about 40% of the total.

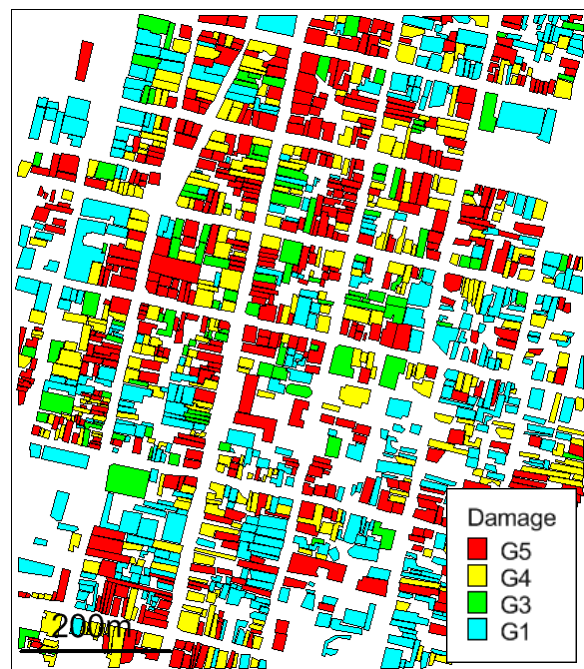


Fig. 2 Building damage data

3. CHARACTERISTICS OF IMAGES IN DAMAGED BUILDINGS

3.1 Image Characteristics

Figure 3 shows the comparison of the pre- and post-event images for each damage level. We can confirm no difference between the images in the G1 building. Also in the G3 building, significant change on the roof and its surroundings between the images is not identified. We can identify debris around the G4 building as shown by an arrow and can estimate that the some part of the building is damaged. However, the difference of the G4 building roof itself between the images is almost indiscernible. In the G5-buildings, on the contrary, the roofs are completely destroyed and the debris produced from the collapsed building materials is scattered in and around the buildings, indicating that it is feasible to identify the collapsed buildings from the images. In this study, we try to automatically detect the G5 buildings through the digital analysis of the images.

When the details of the images in the G5 buildings are carefully examined, the building edges are clearly identified and the homogeneous pixels are distributed on the roofs in the pre-event image. In the post-event image, on the other hand, the bright pixels and dark pixels are densely neighboured each other in the debris area. Since such image change can be analyzed by the image texture, the texture analysis is applied to the images for detecting the collapsed buildings.

3.2 Texture Measures Based on Gray Level Co-Occurrence Matrix

The image texture measures have been proposed such as first-order, second-order and higher-order statistical measures. Since the first order measures such as average and variance are based on the histograms of digital numbers in an image, the relation between neighbouring pixels cannot be evaluated. On the other hand, the second-order measures such as indices based on Gray-Level Co-Occurrence Matrix (GLCM) can evaluate the relation between neighbouring pixels. For the calculation of higher-order measures, many parameters are required and careful selection of appropriate parameters is needed. In this study, the texture analysis based on the GLCM is applied.

Figure 4 illustrates the schematic diagram for the calculation of the GLCM. First, a windowed area is extracted from the image I (see Fig. 4(a)). Next, co-occurrence frequencies of a pair of digital numbers (i and j) for horizontally and vertically neighbouring pixels are calculated and normalized by the number of total pairs (see Fig. 4(b) and (c)). The GLCM is mathematically represented as the following equations;

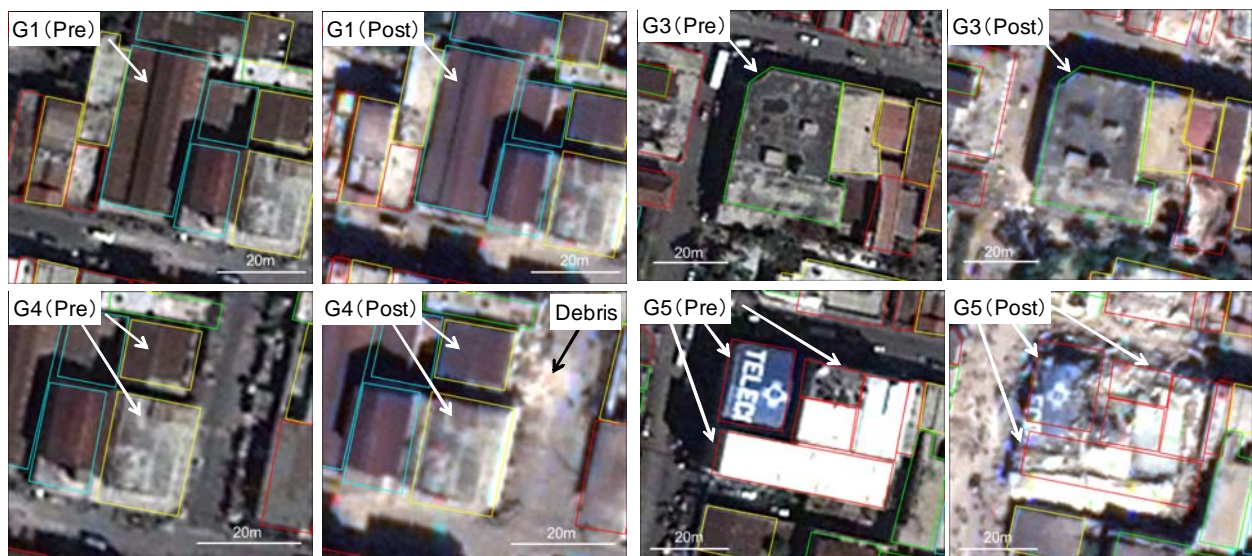


Fig. 3 Comparison of pre- and post-event images for each damage level

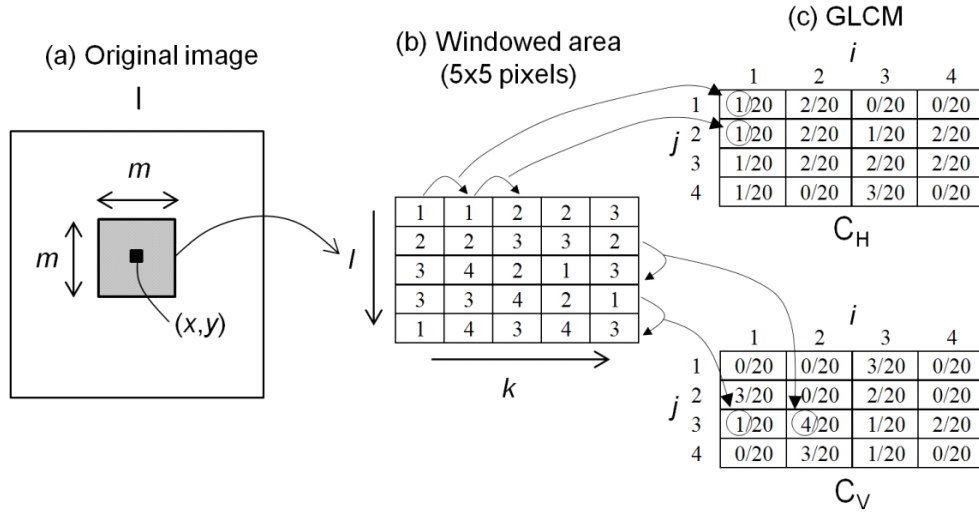


Fig. 4 Schematic diagram for calculation of GLCM

$$C_H(i, j) = \frac{1}{m(m-1)} \cdot \sum_{l=ls}^{le} \sum_{k=ks}^{ke} \begin{cases} 1, & \text{if } I(k, l) = i \text{ and } I(k+1, l) = j \\ 0, & \text{otherwise} \end{cases} \quad (1)$$

$$C_V(i, j) = \frac{1}{m(m-1)} \cdot \sum_{l=ls}^{le} \sum_{k=ks}^{ke} \begin{cases} 1, & \text{if } I(k, l) = i \text{ and } I(k, l+1) = j \\ 0, & \text{otherwise} \end{cases}$$

$$ks = x + (m-1) / 2, \quad ke = x + (m-1) / 2$$

$$ls = y - (m-1) / 2, \quad le = y + (m-1) / 2$$

Here, C_H and C_V indicate the GLCM calculated for horizontally and vertically neighbouring pixels, respectively and m represents a size of the window. Various texture measures based on the GLCM have been proposed (Haralick et al., 1973). In this study, typical texture measures shown below are calculated.

$$UNI = \frac{1}{2} \left(\sum_{i=0}^{255} \sum_{j=0}^{255} C_H(i, j)^2 + \sum_{i=0}^{255} \sum_{j=0}^{255} C_V(i, j)^2 \right) \quad (2)$$

$$ENT = -\frac{1}{2} \left(\sum_{i=0}^{255} \sum_{j=0}^{255} C_H(i, j) \cdot \log(C_H(i, j)) + \sum_{i=0}^{255} \sum_{j=0}^{255} C_V(i, j) \cdot \log(C_V(i, j)) \right) \quad (3)$$

$$CON = \frac{1}{2} \left(\sum_{i=0}^{255} \sum_{j=0}^{255} (i-j)^2 C_H(i, j) + \sum_{i=0}^{255} \sum_{j=0}^{255} (i-j)^2 C_V(i, j) \right) \quad (4)$$

$$DIS = \frac{1}{2} \left(\sum_{i=0}^{255} \sum_{j=0}^{255} |i-j| C_H(i, j) + \sum_{i=0}^{255} \sum_{j=0}^{255} |i-j| C_V(i, j) \right) \quad (5)$$

Here, the equations are for 8-bit image (256 gray tone: 0-255). UNI, ENT, CON and DIS represent

uniformity, entropy, contrast and dissimilarity of the image, respectively. When the homogeneous pixels are concentrated, the image shows larger UNI. When bright pixels and dark pixels are dispersed, the image shows larger ENT. When the bright pixels and dark pixels are neighbored each other, the image shows larger CON and DIS.

Before applying the texture analysis to the images, the resolution of the post-event WV image is resampled to 0.6m to superpose to the pre-event QB image with the resolution of 0.6m. Among the four band images, the red band image is used in the analysis because the reflectance of the debris of masonry buildings in the red band is stronger than in other bands (Miura et al., 2007). Since the

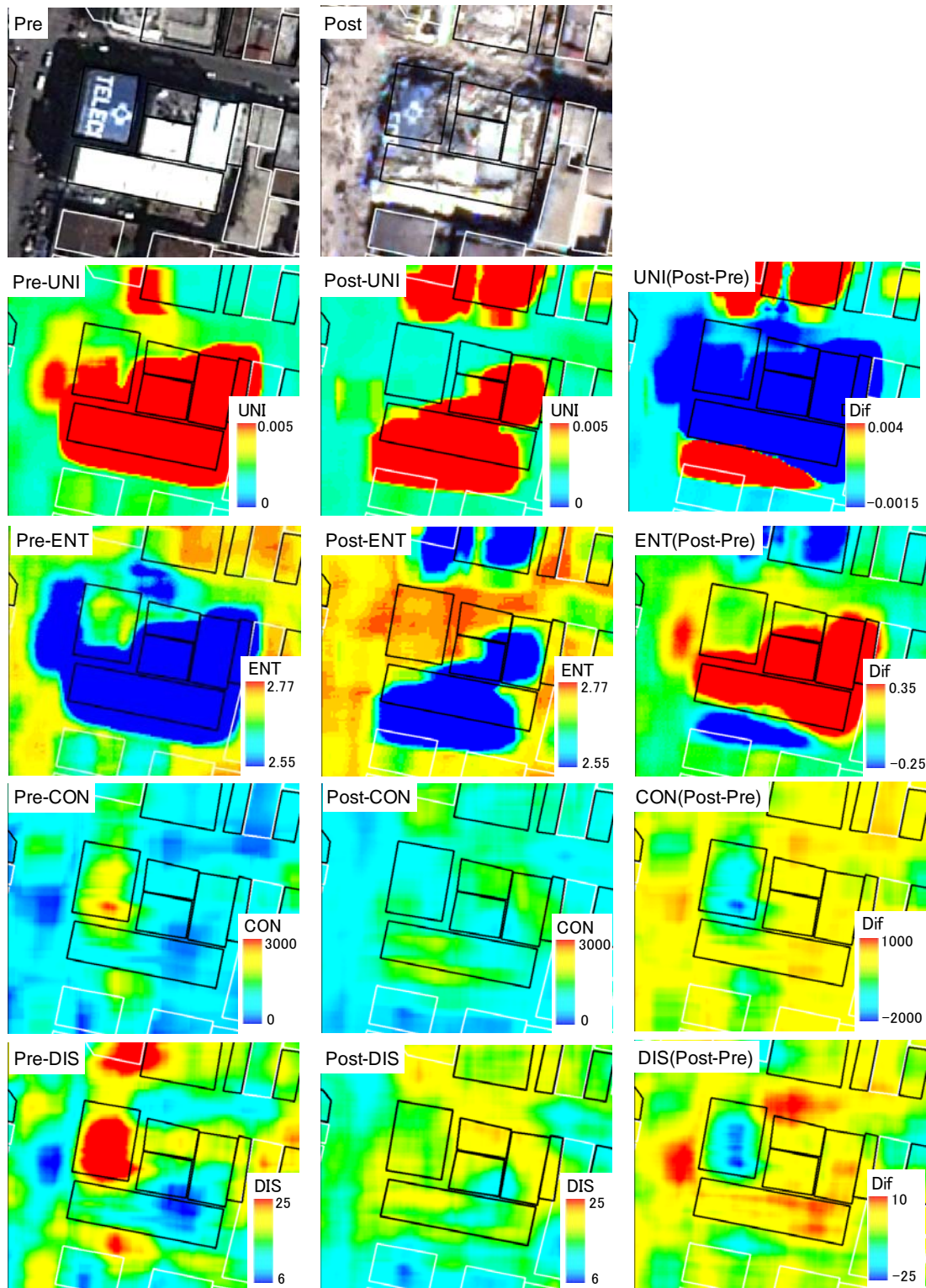


Fig. 5 Distribution of texture measures in collapsed buildings

building size in the target area is about 10 to 20m, we adopt the window size for the GLCM, m , of 25x25 pixels (15x15 m).

Figure 5 shows the comparison of the texture measures in the G5 building shown in Fig. 3. In the rough textured area in the collapsed building, the post-event UNI and ENT are expected to be smaller and larger, respectively. However, the debris area shows larger UNI and smaller ENT because they are sensitive to the bright pixels in the debris. Besides, significant changes between the pre- and post-event UNI and ENT are not identified. On the contrary, the debris area in the post-event image shows larger CON and DIS while the area in the pre-event image shows smaller values, indicating that these indices are better classifier for the building damage detection. Since the change of the pre- and post-event DIS is much clearer than that of CON, we adopt the DIS for the building damage detection in this study.

4. DETECTION OF COLLAPSED BUILDINGS

As discussed above, the high DIS areas in the post-event image would possibly represent the collapsed buildings. However, there are not only flat-roof buildings but also rough-roof buildings such as building with small features on the roof. The post-event DIS would be also large in such rough-roof buildings even if they are not damaged, indicating that it is difficult to detect the collapsed buildings only by using the post-event DIS. To suppress the effect of the rough-roofs, the ratio (Post/Pre) and difference (Post-Pre) of the pre and post-event DIS are calculated. Figure 6 shows a close-up of a rough-roof building, the post-event DIS (PD), the ratio (RD) and the difference (DD). Although the PD values are large in the building area, the values of the RD and DD are suppressed, suggesting that less damaged buildings can be classified more accurately by using not only the PD but also the RD or the DD.

The median values of the PD, RD and DD in each building footprint area are calculated. Figure 7 shows the relations between (a) PD and RD, and (b) PD and DD. Crosses and circles represent G1-G4 buildings and G5 buildings, respectively. Although the values are largely dispersed, the G1-G4 buildings show smaller values and the G5 buildings tend to show larger values. In order to find which index or combination of the indices can more accurately extract the G5 buildings, the axes of Z1-Z5 are defined as shown by solid and dotted lines in Fig. 7 and the values along the axes are calculated. The index Z1, Z2 and Z3 correspond to PD, RD and DD, respectively. The index Z4 and Z5 indicate the combination of PD and RD and the combination of PD and DD, respectively.

ROC (Receiver Operating Characteristics) analysis is applied to the indices for the accuracy assessment of the damage detection. The ROC has been used in signal detection theory to depict the trade-off between hit rates and false alarm of classifiers (Fawcett, 2006). The ROC curve is based on the tow-by-two confusion matrix as shown in Table 1. True Positive Rate (TPR) is calculated as a ratio of number of true positives (TP) divided by number of total positives (P). False Positive Rate (FPR) is calculated as a ratio of number of false positives (FP) divided by number of total negatives (N). A ROC curve is plotted as a relationship between TRP and FPR for various thresholds.

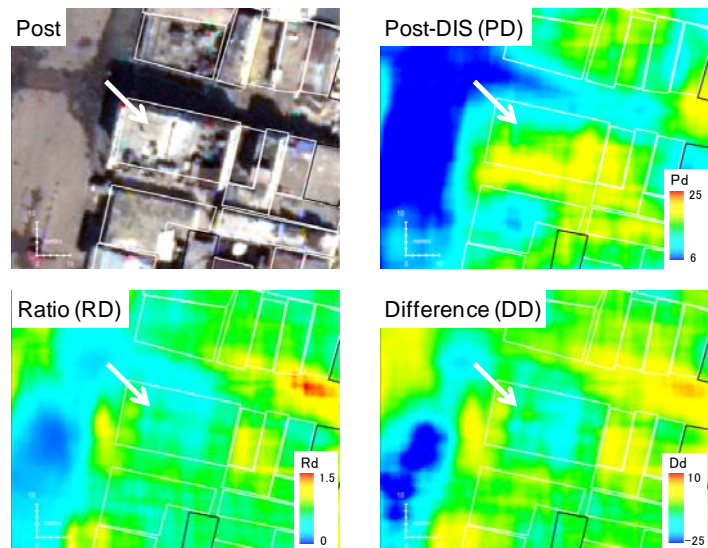


Fig. 6 Comparison of PD, RD and DD

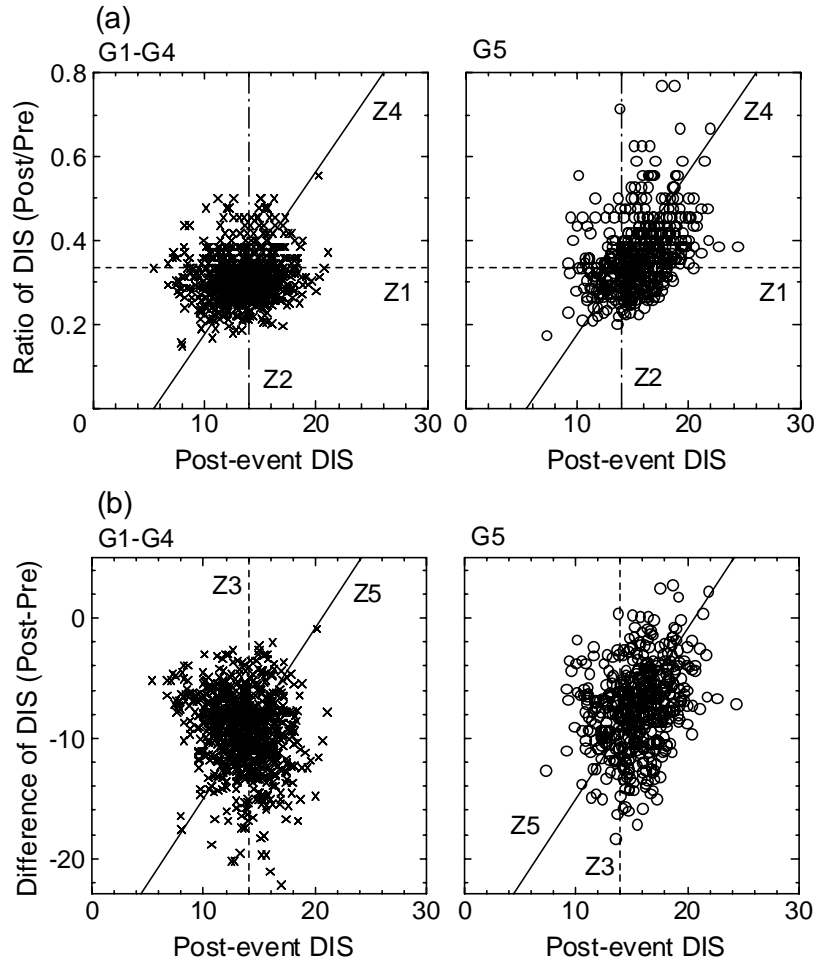


Fig. 7 Relationships between (a) Post-event DIS and Ratio of DIS
(b) Post-event DIS and Difference of DIS

Table 1 Classification for ROC analysis

		Truth (Damage Data)	
		G5	G1-G4
Estimation (Image Analysis)	G5	True Positive (TP)	False Positive (FP)
	G1-G4	False Negative (FN)	True Negative (TN)
Total		P	N
		True Positive Rate = TP/P	False Positive Rate = FP/N

Figure 8 shows the ROC curves for the Z1-Z5 indices. In the ROC graph, the point (0,1) represents perfect classification. If the curve is closer to the point (0,1), the detection accuracy is higher. Among the ROC curves, the Z5 shows higher accuracy than other indices, indicating that the combination of the PD and DD is better classifier for the damage detection. As plotted in the Fig. 8, the TPR and FPR at the Z5 of 6.6 are 0.68 and 0.33, respectively. The distribution of the collapsed buildings is estimated by classifying the buildings whose Z5 values are higher than 6.6 to the G5 buildings. Figure 9 illustrates the comparison of the collapsed buildings between the estimation and the damage data. Many collapsed buildings are correctly detected by the proposed method. Table 2 indicates the number of the G5 and G1-G4 buildings correctly and mis-correctly classified. The result shows that about 70% of the collapsed and less damaged buildings are correctly detected.

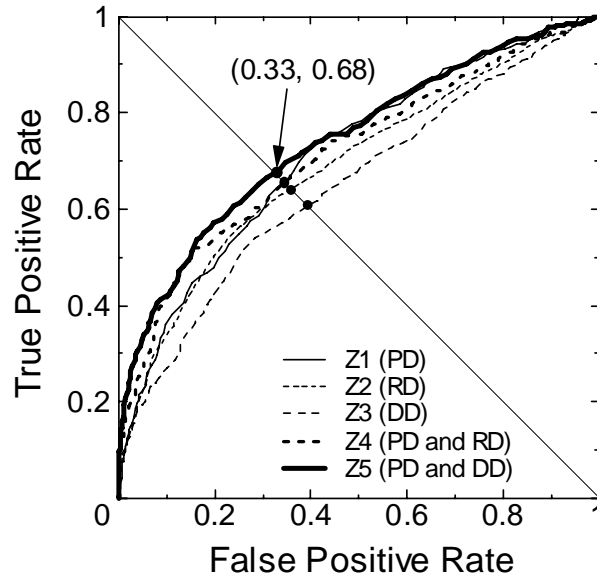


Fig. 8 ROC curves for index Z1 to Z5

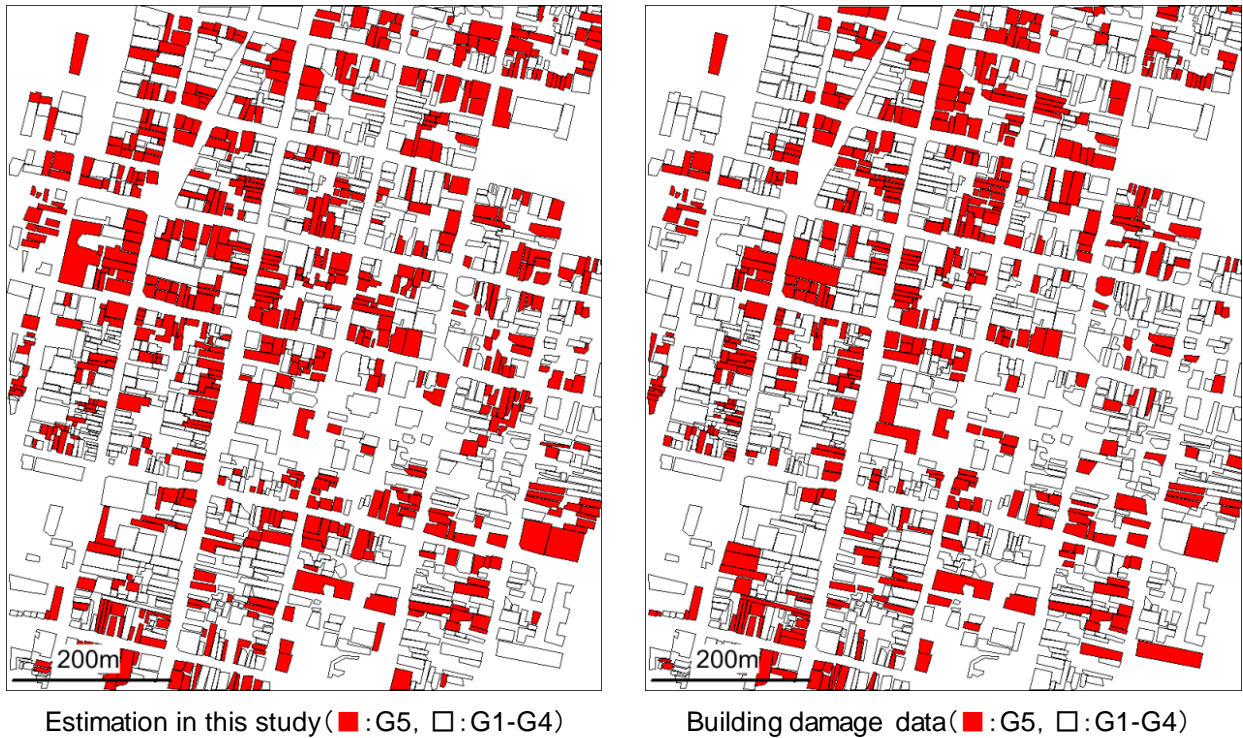


Fig. 9 Distributions of G5 buildings estimated in this study and damage data

Table 2 also indicates that about 30% of the collapsed buildings are mis-detected. To examine the cause of the mis-detections, the G5 buildings are classified to buildings whose roofs are completely destroyed and buildings whose roofs are partially damaged or undamaged in the image. The result of the classification shows that about 90% of the former buildings are correctly detected because the debris produced from the collapsed roofs is widely distributed in the building footprints and they are easily identified by the texture analysis. On the other hand, about 60% of the latter buildings are detected because the debris is distributed in small part or no part of the building roofs. More sophisticated procedure to detect the G5 buildings with partially and undamaged roofs should be examined in order to improve the detection accuracy.

Table 2 Result of accuracy assessment

		Building Dmage Data	
		G5	G1-G4
Estimation by	$Z \geq 6.6$	346	284
Texture analysis	$Z < 6.6$	162	586
Total		508	870
		TPR(%)	FPR(%)
		68.1	32.6

5. CONCLUSIONS

In order to develop a methodology for automatically detecting damaged buildings from satellite images, the characteristics of the damaged areas in the high-resolution satellite images observed before and after the 2010 Haiti earthquake were examined. The image texture in and around the collapsed buildings was significantly roughed in the post-event image because many debris produced from the buildings was observed. From the image texture analysis based on the gray level co-occurrence matrix, the DIS (dissimilarity), one of the texture measures, was identified as better classifier in detecting the collapsed buildings. Based on the ROC analysis, we revealed that the combination of the post-event DIS and the difference of DIS between the pre- and post-event images can provide more accurate result of the damage detection. The result showed that about 70% of the collapsed and less-damaged buildings were correctly classified by the proposed method.

ACKNOWLEDGMENT

A part of this research was conducted in the Global COE program of the MEXT, entitled “International Urban Earthquake Engineering Center for Mitigating Seismic Mega Risk” (Program leader; Prof. Kohji Tokimatsu, Tokyo institute of Technology).

REFERENCES

- Fawcett, T. (2006) An Introduction of ROC Analysis, *Pattern Recognition Letters*, **27**, 861-874.
- Ghosh, S., Huyck, C. K., Greene, M., Gill, S. P., Bevington, J., Svekla, W., DesRoches, R. and Eguchi, R. T. (2011) Crowdsourcing for Rapid Damage Assessment: The Global Earth Observation Catastrophe Assessment Network (GEO-CAN), *Earthquake Spectra*, **27:S1**, S179-S198.
- Government of the Republic of Haiti (2010) *Action Plan for National Recovery and Development of Haiti –Immediate Key Initiatives for the Future-*, [http:// http://www.haiticonference.org/Haiti_Action_Plan_ENG.pdf](http://www.haiticonference.org/Haiti_Action_Plan_ENG.pdf).
- Haralick, R. M., Shanmugam, K. and Dinstein, I. (1973) Textural Features for Image Classification, *IEEE Trans. Systems, Man and Cybernetics*, **SMC-3:6**, 610-621.
- Huyck, C. K., Adams, B. J., Cho, S., Chung, H.-C. and Eguchi, R. T. (2005) Towards Rapid Citywide Damage Mapping Using Neighborhood Edge Dissimilarities in Very High-Resolution Optical Satellite Imagery –Application to the 2003 Bam, Iran, Earthquake–, *Earthquake Spectra*, **21:S1**, S255-S266.
- Miura, H., Yamazaki, F. and Matsuoka, M. (2007) Identification of Damaged Areas due to the 2006 Central Java, Indonesia, Earthquake Using Satellite Optical Images, *Proceedings of 2007 Urban Remote Sensing Joint Event*, Paper No. DIS4.
- Rathje, E. M., Crawford, M., Woo, K. and Neuenchwander, A. (2005) Damage Patterns from Satellite Images of the 2003 Bam, Iran, Earthquake, *Earthquake Spectra*, **21:S1**, S295-S307.
- UNISTAR/UNOSAT, World Bank and EC Joint Research Centre (2010) Joint Remote Sensing Damage Assessment Database, Haiti Earthquake 12 January 2010, In Support to Post Disaster Needs Assessment and Recovery Framework (PDNA), <http://www.unitar.org/unosat/haiti-earthquake-2010-remote-sensing-based-building-damage-assessment-data>.